Robotica (2011) volume 29, pp. 691–703. © Cambridge University Press 2010
doi:10.1017/S0263574710000585

ODE-based obstacle avoidance and trajectory planning for unmanned surface vessels

Reza A. Soltan*, Hashem Ashrafiuon and Kenneth R. Muske

Center for Nonlinear Dynamics and Control, Villanova University, Villanova, PA 19085, USA

(Received in Final Form: September 3, 2010. First published online: October 4, 2010)

SUMMARY

A new method for real-time obstacle avoidance and trajectory planning of underactuated unmanned surface vessels is presented. In this method, ordinary differential equations (ODEs) are used to define transitional trajectories that can avoid obstacles and reach a final desired target trajectory using a robust tracking control law. The obstacles are approximated and enclosed by elliptical shapes. A transitional trajectory is then defined by a set of ordinary differential equations whose solution is a stable elliptical limit cycle defining the nearest obstacle on the vessel's path to the target. When no obstacle blocks the vessel's path to its target, the transitional trajectory is defined by exponentially stable ODE whose solution is the target trajectory. The planned trajectories are tracked by the vessel through a sliding mode control law that is robust to environmental disturbances and modeling uncertainties and can be computed in real time. The method is illustrated using a complex simulation example with a moving target and multiple moving and rotating obstacles and a simpler experimental example with stationary obstacles.

KEYWORDS: Autonomous surface vessels; Trajectory planning; Obstacle avoidance; Navigation; Tracking control.

1. Introduction

Trajectory planning, obstacle avoidance, and position control of underactuated vehicle systems have received increased attention because of technological advances that make fully autonomy a possibility. Unmanned surface vessels (USVs) with two actuator inputs are a type of underactuated vehicle, as they possess more degrees-of-freedom (DOF) than actuator inputs. Consider the planer model of a USV as shown in Fig. 1. The control inputs from the two propellers can only provide a surge motion and planar rotation. The difficulty arises from the fact that only one input (total surge force) will appear in the two nonlinear differential equations representing the planar tracking motion. Hence, tracking a trajectory is only possible with the aid of the yaw rotation. In general, tracking control is only possible if the desired trajectory does not include all three position variables simultaneously. Normally, the USV must track a planar position and the heading angle is indirectly determined to track the desired points. However, the non-holonomic nature of the equations arising from kinematics and dynamics make the trajectory planning and tracking possible through forward motion and heading angle adjustments.[1–8]

An autonomous USV can fulfill a variety of missions and applications that are of increasing interest and an integral part of autonomy is obstacle avoidance. The USV obstacle avoidance algorithm is being developed by accurately creating a world model based on various sensors, such as vision, radar, and nautical charts. Using this world model, the USV can avoid obstacles with the use of a far-field deliberative obstacle avoidance component and a near-field reactive obstacle avoidance component. Specifically, the current focus is to create a robust obstacle avoidance capability and then move on to more advanced behaviors, such as autonomous recovery, in the case of lost communication, target tracking and/or interception, and collaborative operations.[9]

The literature on obstacle avoidance for mobile robots is much richer because they are a more common platform for research and application. They also typically operate at lower speeds with fewer operating constraints. Much of the earlier work in this field is focused on open-loop model predictive control and trajectory optimization. Because finding the desired trajectory and calculating the control action is normally too time-consuming, these methods are not recommended for real-time control, especially in the presence of disturbances.[10,11] There have also been several methods focusing on multi-vehicle problems. Among these are decentralized control approaches, where local control laws are defined for each agent based on local information[12,13] and behavior-based methods simplify the definition of control laws within the decentralized control framework.[14,15] Perhaps, the most promising approach to obstacle avoidance is the potential field method, which has been extensively utilized for mobile robots with static and dynamic obstacles, implemented in real-time experiments,[16–20] and applied with robust controllers, such as sliding mode control law.[21] Many methods have been introduced to avoid the undesirable effects of potential field methods, such as local minima and unwanted repulsive actions. However, some of these effects still persist.

Another more recent, rarely employed approach to obstacle avoidance is the limit cycle-based method. Ellekilde and Perram[22] use limit cycles to generate trajectories for robot manipulators while avoiding obstacles. They define unstable limit cycles as objects of finite size and shape as a way of modeling complex obstacles to be avoided.

* Corresponding author. Email: soltan@vt.edu

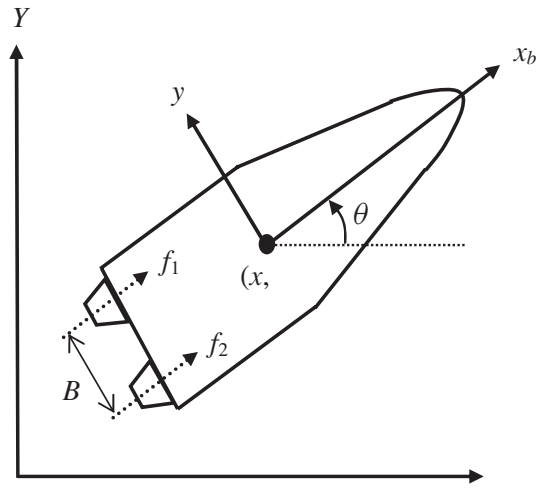

Fig. 1. Planar model of a surface vessel with two propellers.

Use of stable limit cycles as a navigation method has been introduced for obstacle avoidance of mobile robots.[23–25] The approach only considers circular limit cycles for mobile robots of the same size all in close proximity, as it's applied to a robot soccer game. Grech and Fabri integrated the limit cycle navigation method with classical trajectory tracking control scheme. A limitation of the approach in ref. [23] is that the limit cycle equations are defined with constant coefficients, which makes it only suitable for obstacle in close proximity. This is because the exponentially convergent nature of the limit cycle dynamics requires unreasonably high velocities when the robot is far from the limit cycle. Hence, impractical control demand may be required in these cases. Further, these works only consider circular limit cycles suitable for shapes with approximately the same length and width.

A new ordinary differential equation (ODE)-based real-time obstacle avoidance and trajectory planning method for underactuated USV is presented in this work. The method defines transitional trajectories using ODEs in terms of the position feedback variables.[26] At a given time, the obstacles on a straight line path from the USV to its target are detected. The USV then smoothly transitions to a trajectory that approaches the nearest obstacle on its path. The trajectory is defined as a set of two ODEs whose solution is a stable limit cycle in the shape of an ellipse approximating and enclosing the target obstacle. If the obstacle at any time moves away or when the USV goes around the obstacle, the trajectory is then switched to another limit cycle approximating the next obstacle on the USV path. This process continues until all obstacles are cleared and the USV smoothly converges to a transitional target trajectory, which is defined by a set of two exponentially convergent ODEs whose solution is the target trajectory. All transitional trajectories are defined with variable coefficients to yield practical trajectories that can be tracked by a real USV. A sliding mode control law developed for trajectory following the underactuated USV[7] is integrated with the navigation method for robust tracking. The stability of the moving and rotating elliptical limit cycles is established by Lyapunov's stability theorem.[27] Simulation and experimental examples are presented to demonstrate the method's capabilities.

The novelty of the proposed method is in its use of ODEs for trajectory planning and general use of elliptical limit cycles with variable coefficients for smooth and practical trajectory transitions, application of a robust control law to real-time obstacle avoidance for surface vessels, and obstacle avoidance experimentation with surface vessels. The advantages of this method include computational efficiency, robustness, inclusion of moving and rotating obstacles, and small data requirement specifying only current target position and obstacles' approximate size and position.

2. Trajectory Planning Strategy

The planar position tracking transitional trajectory may be described by two ODEs as follows:

$$\dot{x}_i = f_i(x_1, x_2, t), \quad f_i : D_i \to R^2, \quad i = 1, 2, \tag{1}$$

where x_1 and x_2 are the state variables, D_i is an open and connected subset of R^2, and f_i is a locally Lipschitz map from D_i into R^2. In this approach, the transitional trajectory state variables x_1 and x_2 and the form of functions f_1 and f_2 are selected in order to reach a final target trajectory while avoiding both static and dynamic obstacles. Two general forms of the ODEs in Eq. (1) are defined in order to achieve this goal. The first is for reaching the target trajectory and the second for avoiding any obstacles on the USV path. The former is denoted as the *transitional target trajectory* and the later as the *transitional limit cycle trajectory*.

2.1. Transitional target trajectory

The planar position of a USV is defined by the global variables $x(t)$ and $y(t)$, and its target position by $x_t(t)$ and $y_t(t)$. The state variables $x_1(t)$ and $x_2(t)$ of Eq. (1) may be defined as the relative target position:

$$x_1 = x - x_t, \quad x_2 = y - y_t. \tag{2}$$

Therefore, if the ODEs in Eq. (1) are defined such that they have a stable solution, then

$$x_1(t) \,\&\, x_2(t) \to 0 : \quad x(t) \to x_t(t) \,\&\, y(t) \to y_t(t). \tag{3}$$

An example of exponentially stable trajectory is the following linear ODE system:

$$\begin{cases} \dot{x}_1 = -k_1 x_1 & k_1(t) > 0 \\ \dot{x}_2 = -k_2 x_2 & k_2(t) > 0, \end{cases} \quad t \geq t_0, \tag{4}$$

where t_0 is the starting time of the trajectory. The positive parameters $k_1(t)$ and $k_2(t)$ are assumed to be the functions of time in order to generate trajectories that are more desirable and smooth. In general, they are selected as monotonically increasing positive time functions starting from a small value and defined based on the USV's actuator limitations and its distance to the target. These parameters can also be effectively selected based on constrained optimization.[28] Fifth-order polynomials are also good candidates for smooth

https://doi.org/10.1017/S0263574710000585 Published online by Cambridge University Press

and monotonic transition of these functions starting from time t_0 and ending at time t_1. The following polynomial may be used to compute $k_i (i = 1, 2)$ during the transition period $(t_0 \leq t \leq t_1)$:

$$k_i = k_{i5}\Delta t^5 + k_{i4}\Delta t^4 + k_{i3}\Delta t^3 + k_{i2}\Delta t^2 + k_{i1}\Delta t + k_{i0}, \tag{5}$$

where $\Delta t = t - t_0$ and the boundary conditions are selected to smoothly increase k_i from 1% to 100% of its final value $\bar{k}_i$:

$$\begin{aligned} &k_i(t_0) = \bar{k}_i/100, \quad k_i(t_1) = \bar{k}_i, \\ &\dot{k}_i(t_0) = \dot{k}_i(t_1) = \ddot{k}_i(t_0) = \ddot{k}_i(t_1) = 0. \end{aligned} \tag{6}$$

The six polynomial coefficients k_{ij}, $j = 0, \ldots, 5$ are derived using the six boundary conditions specified in Eq. (6). Note that $k_i = \bar{k}_i$ for $t > t_1$ and t_1 is selected based on the initial distance of the target from the vessel.

2.2. Transitional limit cycle trajectory

The obstacle avoidance strategy presented in this work is based on approximating all obstacles as continuously differentiable shapes that can be represented as the limit cycle solution of the ODEs presented in Eq. (1). In this case, the state variables of the transitional trajectory are defined as

$$\begin{aligned} x_1 &= x - x_o, \\ x_2 &= y - y_o, \end{aligned} \tag{7}$$

where $x_o(t)$ and $y_o(t)$ denote the global position of the origin of the limit cycle. The origin of the limit cycle is assumed to be a function of time to allow for dynamic obstacles. Consider a limit cycle of the form $\ell(x_1, x_2, t)$, which may also be an explicit function of time to account for obstacle planar rotation. Thus, the transitional limit cycle trajectory will have the following special form:

$$\begin{cases} \dot{x}_1 = h_1(x_1, x_2, t) - k_1 x_1 \ell(x_1, x_2, t) & k_1(t) > 0, \\ \dot{x}_2 = h_2(x_1, x_2, t) - k_2 x_2 \ell(x_1, x_2, t) & k_2(t) > 0. \end{cases} \tag{8}$$

The functions $h_1(x_1, x_2, t)$ and $h_2(x_1, x_2, t)$ represent the planar particle motion kinematics at the limit cycle, i.e., when $\ell(x_1, x_2, t) = 0$. The solution of Eq. (8) must guarantee that a USV starting from any point outside the limit cycle where $\ell(x_1, x_2, t) > 0$ will converge to the limit cycle without crossing it. The positive parameters $k_1(t)$ and $k_2(t)$ are again assumed to be the functions of time in order to generate more desirable smooth trajectories using Eq. (5).

2.3. Elliptical limit cycles

The limit cycle geometry considered in this work is elliptical because it can be used to closely approximate convex vessel shapes. When two or more obstacles collide or are in close contact to each other, they can be approximated as a single obstacle and enclosed by a larger ellipse. Note that if an object does not have a convex shape, it is still more efficient to approximate it with an ellipse for the purpose of obstacle avoidance except in cases where the target is hiding inside the concave part of the object. In these cases, the limit cycle may be defined as a cross section of ellipses approximating the concave shape.

The limit cycle $\ell(x_1, x_2, t)$ is defined by the general equation of an ellipse with semi-major and semi-minor axes, a and b, respectively, and origin at $(x_o(t), y_o(t))$:

$$\begin{aligned} \ell \equiv &\left[\frac{\cos\phi x_1 + \sin\phi x_2}{a}\right]^2 \\ &+ \left[\frac{-\sin\phi x_1 + \cos\phi x_2}{b}\right]^2 - 1 = 0, \end{aligned} \tag{9}$$

where $x_1(t)$ and $x_2(t)$ are defined in Eq. (7) and $\varphi(t)$ is the angle representing the orientation of the ellipse's semi-major axis relative to the global horizontal axis. This angle can be time-dependent to represent rotating objects. The motion of a particle with angular speed $\Omega(t)$ around an ellipse rotating with angle $\phi(t)$ and a moving origin at $(x_o(t), y_o(t))$ may be given as

$$\begin{cases} x_1 = a\cos\phi\cos\Omega t - b\sin\phi\sin\Omega t, \\ x_2 = a\sin\phi\cos\Omega t + b\cos\phi\sin\Omega t. \end{cases} \tag{10}$$

The time derivative of Eq. (10) may be written as

$$\begin{cases} \dot{x}_1 = -(\Omega + \dot{\Omega}t)(a\cos\phi\sin\Omega t + b\sin\phi\cos\Omega t) - x_2\dot{\phi}, \\ \dot{x}_2 = (\Omega + \dot{\Omega}t)(-a\sin\phi\sin\Omega t + b\cos\phi\cos\Omega t) + x_1\dot{\phi}, \end{cases} \tag{11}$$

where $\dot{\Omega}$ is the time derivative of $\Omega(t)$. Note that $\Omega(t) > 0$ and $\Omega(t) < 0$ represent counterclockwise (CCW) and clockwise (CW) rotation of the particle, respectively. In addition, $\Omega(t)$ is assumed to be increasing monotonically in magnitude such that $\Omega + \dot{\Omega}t \neq 0$. Again, a fifth-order polynomial is used to transition $\Omega(t)$ from 1% to 100% of its final constant value $\bar{\Omega}$ in the selected transition period of $t_0 \leq t \leq t_1$:

$$\Omega = \Omega_5\Delta t^5 + \Omega_4\Delta t^4 + \Omega_3\Delta t^3 + \Omega_2\Delta t^2 + \Omega_1\Delta t + \Omega_0, \tag{12}$$

where $\Delta t = t - t_0$ and the six polynomial coefficients, Ω_i, $i = 0, \ldots, 5$, are derived based on the six boundary conditions:

$$\begin{aligned} &\Omega(t_0) = \bar{\Omega}/100, \quad \Omega(t_1) = \bar{\Omega}, \\ &\dot{\Omega}(t_0) = \dot{\Omega}(t_1) = \ddot{\Omega}(t_0) = \ddot{\Omega}(t_1) = 0. \end{aligned} \tag{13}$$

Eliminating $\cos\Omega t$ and $\sin\Omega t$ from Eqs. (10) and (11), we get

$$\begin{cases} \dot{x}_1 = -x_2\dot{\phi} + \dfrac{\Omega + \dot{\Omega}t}{ab}(h_{e11}x_1 - h_{e12}x_2), \\ \dot{x}_2 = +x_1\dot{\phi} + \dfrac{\Omega + \dot{\Omega}t}{ab}(h_{e21}x_1 - h_{e11}x_2), \end{cases} \tag{14}$$

https://doi.org/10.1017/S0263574710000585 Published online by Cambridge University Press

where

$$\begin{aligned} h_{e11} &= (a^2 - b^2)\sin\phi\cos\phi, \\ h_{e12} &= a^2\cos^2\phi + b^2\sin^2\phi, \\ h_{e21} &= b^2\cos^2\phi + a^2\sin^2\phi. \end{aligned} \tag{15}$$

The functions $h_1(x_1, x_2, t)$ and $h_2(x_1, x_2, t)$ in Eq. (8) for elliptical limit cycles are based on the dynamics represented in Eq. (14) as

$$\begin{cases} h_1(x_1, x_2, t) = -x_2\dot{\phi} + \dfrac{\Omega + \dot{\Omega}t}{ab}(h_{e11}x_1 - h_{e12}x_2), \\ h_2(x_1, x_2, t) = +x_1\dot{\phi} + \dfrac{\Omega + \dot{\Omega}t}{ab}(h_{e21}x_1 - h_{e11}x_2). \end{cases} \tag{16}$$

2.4. *The obstacle avoidance algorithm*

Consider a USV trying to catch a dynamic target with multiple dynamic obstacles in its vicinity. It is assumed that the USV can achieve velocities larger than the target at any point on the moving and rotating obstacles and that the approximate size and location of all obstacles are known to the USV through, for example, a vision-based detection system. All obstacles are approximated as ellipses and the information listed in Table I is assumed to be available at the current time t. When obstacle i is determined to be in the path of the USV, a transitional limit cycle trajectory of the form in Eq. (8) is generated to determine the path around it:

$$\begin{cases} \dot{x}_1(i) = h_1(x_1(i), x_2(i), t) - k_1(i)x_1(i)\ell(x_1(i), x_2(i), t), \\ \dot{x}_2(i) = h_2(x_1(i), x_2(i), t) - k_2(i)x_2(i)\ell(x_1(i), x_2(i), t), \end{cases} \tag{17}$$

Table I. Obstacle position, size, and orientation for $i = 1$ to n.

N	Number of obstacles.
$x_o(i, t)$	Global x position from the center of obstacle i.
$y_o(i, t)$	Global y position of the center of obstacle i.
$a(i)$	Semi-major axis of the ellipse enclosing obstacle i.
$b(i)$	Semi-minor axis of the ellipse enclosing obstacle i.
$\varphi(i, t)$	Orientation angle of the ellipse enclosing obstacle i.

where

$$x_1(i) = x - x_o(i), \quad x_2(i) = y - y_o(i). \tag{18}$$

To explain the algorithm, we borrow from the ideas presented in ref. [23]. Consider a simple case where a USV is commanded to catch a target moving at a constant speed on a horizontal line with two static obstacles blocking its path and a third one away from the path, as shown in Fig. 2. The trajectory generation algorithm is described below and graphically visualized in Fig. 2, where numbers 1 through 4 indicate four "frames" at different times during the tracking.

Step 1. All obstacles in the vicinity of the vessel and the target, as well as of the target position are identified. The obstacles are approximated and enclosed by ellipses (Eq. (9)) based on their size, orientation, and location.

Step 2. The obstacles on the vessel's path to the target are identified using the intersection points between the straight line from the vessel to the target and the ellipses. The equation

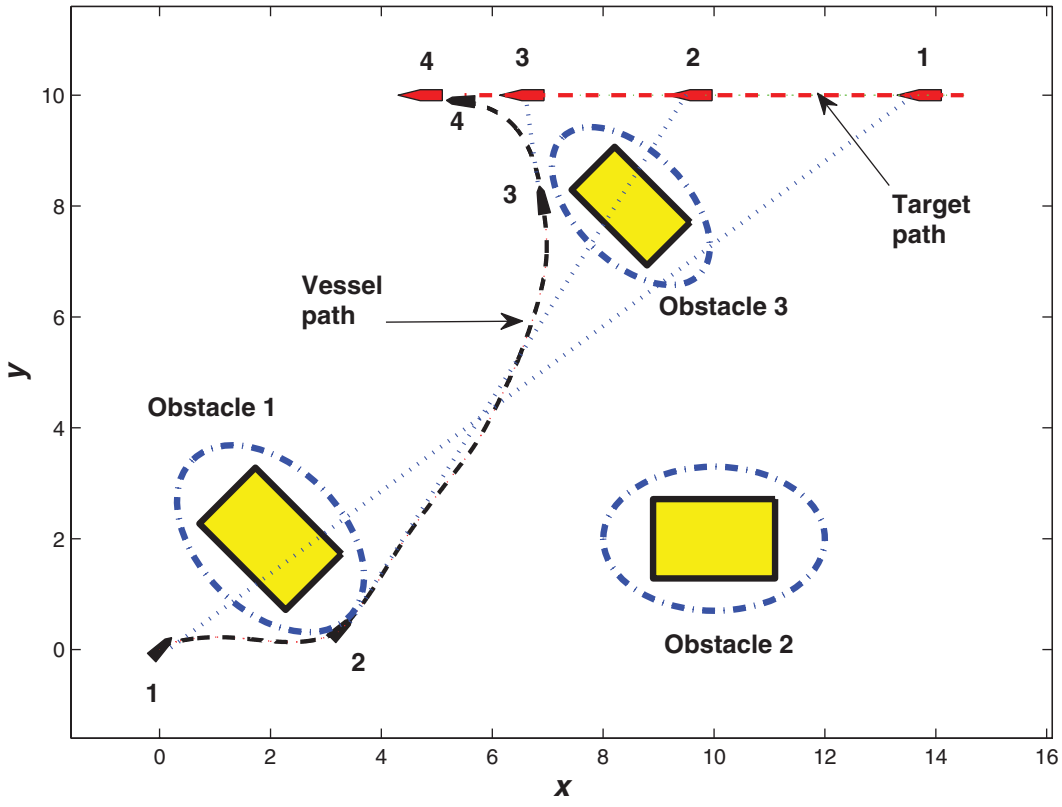

Fig. 2. Conceptual demonstration of the obstacle avoidance algorithm.

https://doi.org/10.1017/S0263574710000585 Published online by Cambridge University Press

of the straight line $l(t)$ is given by

$$l(t) : y_l = y_t + \frac{y - y_t}{x - x_t}(x_l - x_t), \tag{19}$$

where $x_l(t)$ and $y_l(t)$ are the two variables of the planar straight line path. All obstacles, which do not have any intersection with the straight line, are ignored now. In this example, the straight line from the vessel to the target at the initial position (step 1) intersects with obstacles 1 and 3 as shown in Fig. 2.

Step 3. The obstacle closest to the vessel is identified and a transitional limit cycle trajectory based on Eq. (8) is generated. The sign of $\omega(t)$ is selected based on the shortest path around the obstacle toward the target using the location of the intersection points with respect to the center of the ellipse and the velocity of the obstacle relative to the target. For our example, obstacle 1 is selected with a positive $\omega(t)$ for CCW rotation, as shown in the path from frame 1 to 2.

Step 4. The vessel tracks the selected transitional limit cycle trajectory while repeating steps 2 and 3 until a new obstacle is detected on its path to the target. For the example shown in Fig. 2, obstacle 3 is detected at frame number 2. The vessel targets a new transitional limit cycle trajectory enclosing obstacle 3. The new path is displayed from frame 2 to 3. Note that obstacle 2 continues to be ignored, as the straight line from the vessel to the target never intersects the ellipsoid approximating its shape.

Step 5. When all obstacles are cleared, the trajectory defined in Eq. (4) is used to catch the target. In this example, the vessel detects the target at frame 3. The final path from frame 3 to 4 is shown in Fig. 2, where the vessel catches the target. Note that all these steps are repeated at every sample time to account for dynamic obstacles. If any obstacle moves to block the path of the vessel to its target, the trajectory transitions back to the limit cycle enclosing that obstacle.

Remark 1. The intersections of the straight line from the vessel to the target and the ellipses defining the obstacles are derived by letting $x = x_l$ and $y = y_l$ in Eq. (7) and substituting from Eqs. (7) and (19) into Eq. (9) for each obstacle. The result is a quadratic equation in x_l. If this equation has real roots within the range defined by the USV and the target, then the obstacle is blocking the vessel path. If there are multiple intersections, then the one closest to the vessel ($\min \sqrt{(x - x_l)^2 + (y - y_l)^2}$) is used to define the new transitional limit cycle.

Remark 2. When the USV moves from one limit cycle to another, the continuity of its trajectory must be maintained. Fifth-order polynomials presented in Eq. (5) can be used to maintain trajectory continuity at position, velocity, and acceleration levels. In general, we can redefine Eq. (1) for the transition period as

$$\dot{x}_i = f_i(x_1, x_2, t) + g_i(t) \quad \text{for} \quad t_0 \le t \le t_1, \quad i = 1, 2, \tag{20}$$

$$g_i = g_{i5}\Delta t^5 + g_{i4}\Delta t^4 + g_{i3}\Delta t^3 + g_{i2}\Delta t^2 + g_{i1}\Delta t + g_{i0}, \tag{21}$$

where $\Delta t = t - t_0$ and the boundary conditions are selected to monotonically transition g_i and its first and second time derivatives to a zero value:

$$\begin{aligned} &g_i(t_0) = \dot{x}_i(t_0) - f_i(t_0), \quad \dot{g}_i(t_0) = \ddot{x}_i(t_0) - \dot{f}_i(t_0), \\ &\ddot{g}_i(t_0) = \dddot{x}_i(t_0) - \ddot{f}_i(t_0), \quad g_i(t_1) = \dot{g}_i(t_1) = \ddot{g}_i(t_1) = 0. \end{aligned} \tag{22}$$

2.5. *Trajectory stability analysis*

The stability of the transitional trajectories proposed in this work is presented in this section.

***Lemma* 1**. The trajectories defined by Eqs. (7)–(9) and (16) asymptotically converge to stable elliptical limit cycles for the set $\{x_1, x_2 \in \ell(x_1, x_2, t) > 0\}$.

Proof: Consider the following positive definite Lyapunov candidate function in the set $\{x_1, x_2 \in \ell(x_1, x_2, t) > 0\}$

$$V(x_1, x_2) = \frac{a^2 b^2}{2}\ell(x_1, x_2, t) > 0. \tag{23}$$

Taking the time derivative of Eq. (23) and substituting from Eqs. (9), (14)–(16):

$$\begin{aligned} \dot{V}(x_1, x_2) = &-k_1\ell(x_1, x_2, t)\left[h_{e21}x_1^2 - h_{e11}\, x_1 x_2\right] \\ &- k_2\ell(x_1, x_2, t)\left[(h_{e12}x_2^2 - h_{e11}\, x_1 x_2\right]. \end{aligned}$$

To prove that the time derivative of the Lyapunov candidate function is negative, let $k_1 = k_2 = k(t) > 0$:

$$\begin{aligned} \dot{V}(x_1, x_2) = &-k\ell(x_1, x_2, t)\left[a^2(-\sin\phi\, x_1 + \cos\phi\, x_2)^2\right. \\ &\left. + b^2(\cos\phi\, x_1 + \sin\phi\, x_2)^2\right] < 0, \end{aligned} \tag{24}$$

which demonstrates stability for $\ell(x_1, x_2, t) > 0$. Note that $V(x_1, x_2) = \dot{V}(x_1, x_2) = 0$, when $\ell(x_1, x_2, t) = 0$. Also note that $k_1 = k_2$ is not required for the special case of circular limit cycles.

***Lemma* 2.** The transitional target trajectory represented by Eq. (4) is exponentially stable.

Proof: This is easily proven by selecting the following Lyapunov candidate:

$$V(x_1, x_2) = \frac{1}{2}\left(x_1^2 + x_2^2\right) > 0,$$

where, using Eq. (4), the time derivative is derived to be negative definite:

$$\dot{V}(x_1, x_2) = -k_1 x_1^2 - k_2 x_2^2 < 0.$$

Further, when k_1 and k_2 reach their constant values after the transition time (see Eq. (5)), solution for Eq. (4) becomes exponentially convergent.

Remark 3. The limit cycle trajectories are asymptotically stable. However, the vessel is only required to remain on each trajectory for a finite amount of time. This is because the vessel moves out of its current limit cycle trajectory as

https://doi.org/10.1017/S0263574710000585 Published online by Cambridge University Press

soon as the obstacle is cleared, as explained and demonstrated in the obstacle avoidance algorithm and the example given in Fig. 2.

Remark 4. All trajectories starting from the inside of the limit cycle with the exception of the origin will also converge to the limit cycle. These cases, however, are not of interest for obstacle avoidance problems considered in this work.

Theorem 1. The trajectory defined in the obstacle avoidance algorithm asymptotically converges to its final target. *Proof:*

The USV follows transitional limit cycle trajectories as along as obstacles block its straight line path to the target and the limit cycle trajectories are asymptotically stable according to Lemma 1. As only obstacles on the direct path to the target are used and the USV is assumed to be faster than all obstacles and the target, the distance to the target will decrease when the vessel moves from one limit cycle to another according to Remark 1. Moving from one transitional trajectory to the next is achieved in finite time according to Remark 3. Hence, the final transitional target trajectory is achieved in finite time and this trajectory reaches the target exponentially according to Lemma 2.

3. Controller Design

The difficulty in the USV control arises from the fact that the state variables of the desired trajectory are not directly controlled but are related to the controlled variables through non-holonomic constraints. Further, the planar model of the USV has three DOF. Hence, a USV with two propellers or a propeller and a rudder is an underactuated system. The body-fixed reference frame velocities are related to global velocities of the USV model shown in Fig. 1 as follows:

$$\begin{aligned} \dot{x} &= v_x \cos\theta - v_y \sin\theta, \\ \dot{y} &= v_x \sin\theta + v_y \cos\theta, \\ \dot{\theta} &= \omega, \end{aligned} \tag{25}$$

where θ represents the vessel orientation, $\dot{x}$, $\dot{y}$, and $\dot{\theta}$ are globally linear and angular velocities, v_x and v_y are its forward and lateral velocities, and ω is the local angular velocity.

The nonlinear differential equations of motion of the USV in the body-fixed reference frame are as follows:

$$\begin{aligned} &m_{11}\dot{v}_x - m_{22}v_y\omega + d_{11}v_x^{\alpha_1} = f, \\ &m_{22}\dot{v}_y + m_{11}v_x\omega + d_{22}\mathrm{sgn}(v_y)|v_y|^{\alpha_2} = 0, \\ &m_{33}\dot{\omega} + m_d v_x v_y + d_{33}\mathrm{sgn}(\omega)|\omega|^{\alpha_3} = T, \end{aligned} \tag{26}$$

where $m_d = m_{22} - m_{11}$ and $m_{22} \neq m_{11}$. Note that only forward motion dynamics are considered. The surge force f and the yaw moment T are derived in terms of the two propellers, f_1 and f_2 as $f = f_1 + f_2$ and $T = (f_2 - f_1)B/2$. For details regarding the USV model derivation, the reader is referred to ref. [1]. Details on the determination of the model parameters can be found in refs. [7, 29].

The control law developed for this work is based on the sliding mode approach[30,31] where a set of two asymptotically stable surfaces, S_1 and S_2, are defined as a function of the body-fixed velocity tracking errors such that all system trajectories converge to these surfaces in finite time and slide along them until they reach the desired destination at their intersection. The reaching conditions are established by defining $\frac{1}{2}(S_1^2 + S_2^2)$ as the Lyapunov function and ensuring that for each surface i[32]

$$S_i\dot{S}_i \leq -\eta_i |S_i|, \quad \eta_i > 0, \quad i = 1, 2, \tag{27}$$

where the value of the constant η_i (effort parameters) determine how fast the trajectory will reach the surface i.

3.1. Surge control law

The first sliding surface is a first-order one and is defined in terms of the vessel's surge motion tracking error

$$S_1 = \tilde{v}_x + \lambda_1 \int_0^t \tilde{v}_x(\tau)d\tau, \tag{28}$$

where "$\sim$" is used to denote the tracking errors, which is the difference between the actual (v_x) and desired (v_{xd}):

$$\tilde{v}_x = v_x - v_{xd}. \tag{29}$$

The desired values are computed from the transitional trajectories presented in Eqs. (1)–(22) and (25).

Taking the time derivative of the surface and using the first relationship in Eq. (26), the surge control input can be determined as

$$f = f_x - k_x sat(S_1/\varphi_1), \tag{30a}$$

$$sat(S_1/\varphi_1) = \begin{cases} S_1/\varphi_1 & \text{if} \quad |S_1| \leq \varphi_1 \\ \mathrm{sgn}(S_1) & \text{if} \quad |S_1| > \varphi_1, \end{cases} \tag{30b}$$

where φ_1 is the boundary layer thickness introduced to eliminate chattering normally associated with sliding mode control. The terms

$$\begin{aligned} f_x &\equiv f_x(v_x, v_y, \omega, v_{xd}, \dot{v}_{xd}), \\ k_x &\equiv k_x(v_x, v_y, \omega, v_{xd}, \dot{v}_{xd}) \end{aligned} \tag{31}$$

are derived based on the nominal model and its uncertainty bounds as presented in ref. [7]. Note that the wave and wind forces may also be modeled[1] with their uncertainties and accounted for in Eq. (32).

3.2. Lateral motion control law

The second sliding surface is a second-order one and is defined in terms of the vessel's lateral motion tracking errors,

$$S_2 = \dot{\tilde{v}}_y + 2\lambda_2\tilde{v}_y + (\lambda_2)^2 \int_0^t \tilde{v}_y(\tau)d\tau, \tag{32}$$

where

$$\tilde{v}_y = v_y - v_{yd}, \quad \dot{\tilde{v}}_y = \dot{v}_y - \dot{v}_{yd}. \tag{33}$$

Taking the time derivative of the lateral equation of motion in Eq. (26) and substituting it into the time derivative of the

https://doi.org/10.1017/S0263574710000585 Published online by Cambridge University Press

Table II. The USV model parameters in SI units.

$m_{11} = 1.956$	$m_{22} = 2.405$	$m_{33} = 0.043$
$d_1 = 2.436$	$d_2 = 12.992$	$d_3 = 0.0564$
$\alpha_1 = 1.510$	$\alpha_2 = 1.747$	$\alpha_3 = 1.592$

second surface yields the following yaw moment control:

$$T = f_y - k_y \text{sat}(S_2/\varphi_2), \tag{34}$$

where the saturation function with boundary layer thickness φ_2 is defined similar to Eq. (30b) and the terms

$$\begin{aligned} f_y &\equiv f_y(v_x, v_y, \omega, v_{xd}, v_{yd}, \dot{v}_{xd}, \dot{v}_{yd}, \ddot{v}_{yd}, f), \\ k_y &\equiv k_y(v_x, v_y, \omega, v_{xd}, v_{yd}, \dot{v}_{xd}, \dot{v}_{yd}, \ddot{v}_{yd}, f) \end{aligned} \tag{35}$$

are derived based on the nominal model and its uncertainty bounds, as presented in ref. [7]. Note that all velocity and acceleration data are assumed to be approximated using an extend Kalman filter[33] or backward difference method.

Remark 5. The control law only guarantees reaching the sets $|S_1| \le \varphi_1$ and $|S_2| \le \varphi_2$, which is associated with a small error depending on the boundary layer thicknesses.[32]

Remark 6. Tracking control of a vessel following the transitional trajectories is very robust because $x(t)$ and $y(t)$ positions are measured and used as feedback in the generation of the trajectory. Hence, if a vessel is thrown off the trajectory by an unexpected large disturbance, it will simply follow a new transitional trajectory starting from its new state.

Remark 7. It is assumed that the vessel is capable of speeds and maneuverings faster than all obstacles and its target.

4. Examples

Our experimental USV, which is .45-m long and weighs 1.614 kg, is used for the examples presented in this section. The USV has two propellers, which are $B = .07$-m apart and are rotated by DC motors. The model parameters identified for the system are shown in Table II in SI units.[29]

4.1. Simulation example

We consider a simulation example, where the USV is commanded to closely follow a moving target in a relatively cluttered environment with moving and rotating obstacles. The target starts at the same position and moves at a constant velocity of .08 m/s up in case 1 and down in case 2. The coordinates of the moving target in the first and second scenarios are defined as

$$\begin{aligned} \text{Case1}: &\quad x_t(t) = 11, \quad y_t(t) = .08t + 10, \\ \text{Case2}: &\quad x_t(t) = 11, \quad y_t(t) = -.08t + 10. \end{aligned}$$

The vessel position is initially at the origin heading 60° above the horizontal. There are four dynamic obstacles crowding the environment and blocking its direct path to the target. The four obstacles are assumed to be moving at constant speed and rotating at a constant angular velocity. The obstacle data are presented in Table III. A period of .2 s is selected for all interpolations required for smooth transition from one trajectory to the next. The trajectory parameters, $\bar{k}_1 = \bar{k}_2 = .04$ and $\bar{\Omega} = .05$, are chosen for all limit cycle trajectories, while $\bar{k}_1 = \bar{k}_2 = .25$ have been selected for the transitional target trajectory. The sliding mode control parameters are selected as $\eta_1 = \eta_2 = 1$, and $\lambda_1 = \lambda_2 = 2$ for both cases. The saturation function boundary layer thicknesses are selected to be $\varphi_1 = \varphi_2 = .1$ to avoid chattering. The propeller forces are saturated at 2.2 N.

Table III. Simulation example obstacle size, position, and motion data.

	Obstacle #1	Obstacle #2	Obstacle #3	Obstacle #4
x_o	8	5	4	2
$\dot{x}_o$	−0.008	0.02	−0.008	0.005
y_o	8	4	8	3
$\dot{y}_o$	0.01	0.02	0.005	0.008
a	1.75	1.5	2	2
b	1	1	1.25	1
ϕ_o	$-\pi/6$	$-\pi/6$	0	$\pi/2$
$\dot{\phi}_o$	−0.005	−0.005	0.008	−0.003

The simulations are run for 90 s in both scenarios and partial frame-by-frame results are displayed in Figs. 3 and 4, where the USV is able to catch the target while passing safely through the field of moving obstacles. The frames shown in the first case (Fig. 3) are for initial and final times and the instances where the transitional trajectories changed are

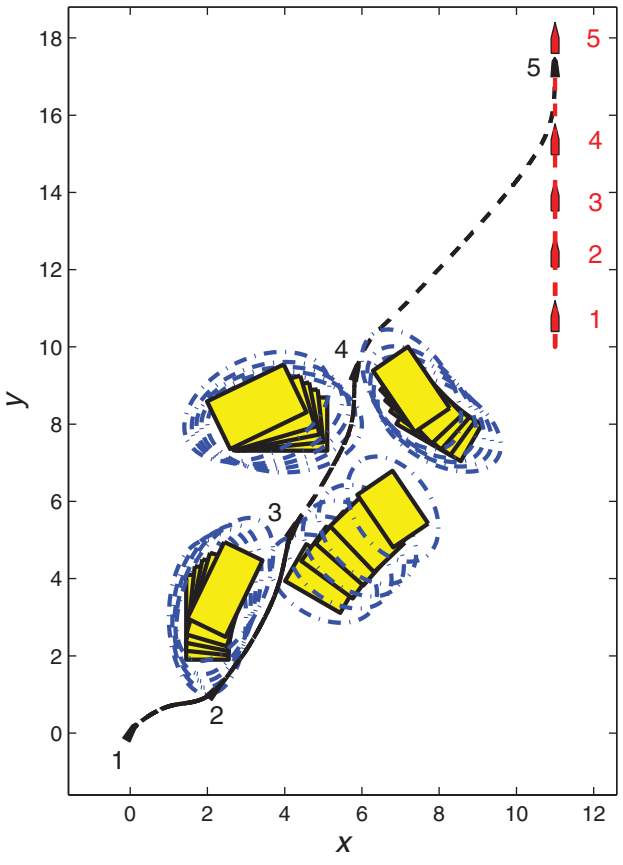

Fig. 3. Reaching and following a moving target through dynamic obstacles during the first scenario.

https://doi.org/10.1017/S0263574710000585 Published online by Cambridge University Press

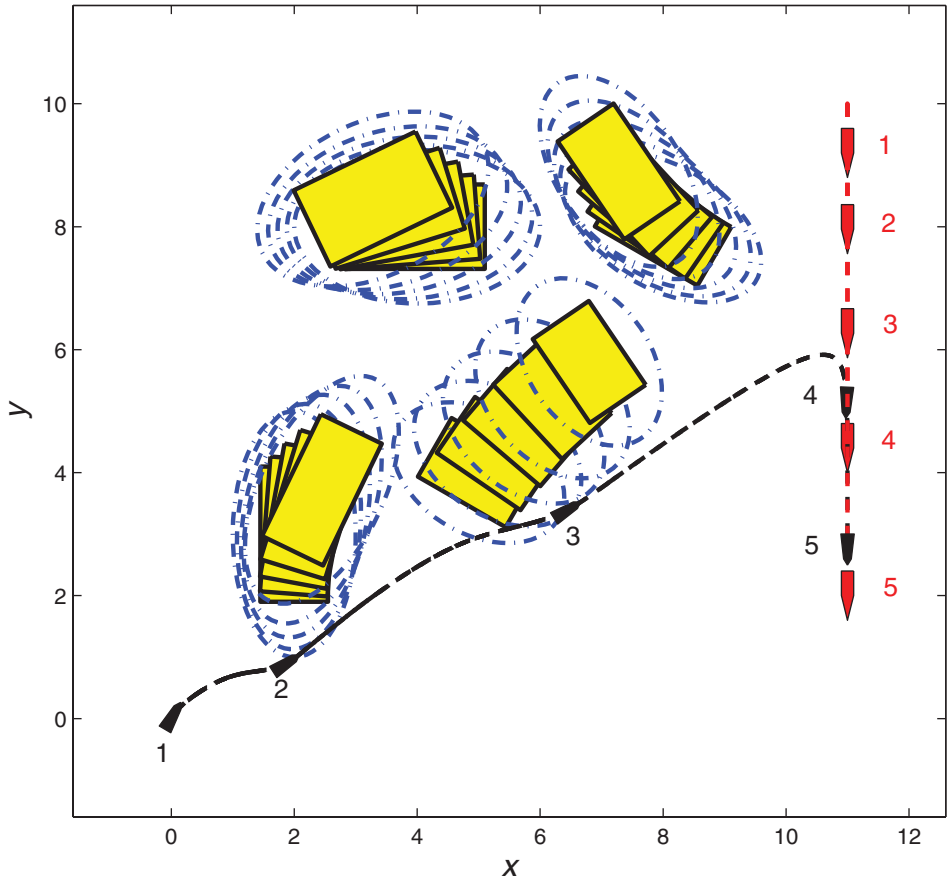

Fig. 4. Reaching and following a moving target through dynamic obstacles during the second scenario.

21.35 s, 39.35 s, and 57.24 s. The frames shown in the second case (Fig. 4) are for initial and final times, the instances where the transitional trajectories are changed at 17.20 s and 37.19 s, and an additional frame after 60 s, where the target has already been reached.

The USV has no prior knowledge of the movements of the target or obstacles in the two cases. Yet it takes two very different paths even though the two cases are identical with the exception of target heading. As new target and obstacle information is received, the algorithm is able to plan shorter and more suitable transitional trajectories such that the first case has four transitional trajectories and the second case has only three. In the first case, the vessel is able to go through tight spaces in-between the obstacle changing from CCW to CW motion and vice versa. However, in the second case the vessel ignores two of the obstacles and goes around the other two.

Figure 5 presents the distance of the USV to the target for two scenarios. In each case, the distance is reduced quickly at the beginning of each transitional trajectory until the USV is close to or on the limit cycle. This is due to the exponentially convergent nature of the transitional trajectories represented by Eqs. (4) and (8). In the first case, the USV is able to catch the target after about 80 s. In the second case it takes less than 60 s because there is one less transitional trajectory and a shorter path is planned. Similarly, the forward velocity in both cases is very large at the beginning of each transition accompanied by abrupt changes in lateral velocity, thereby indicating an oscillatory motion, as shown in Figs. 6 and 7 for

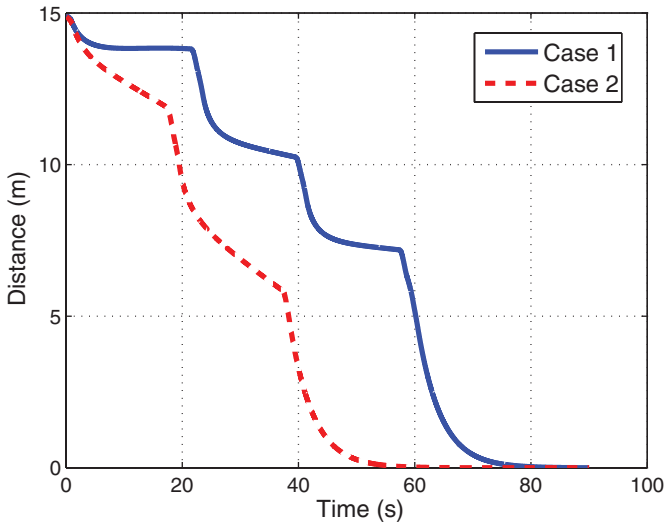

Fig. 5. The time history of the convergence of distance between the USV and its target.

the two cases. Note that the vessel velocity and acceleration are continuous despite the sharp changes, as shown in the enlarged area of each figure. Abrupt changes in the velocities and accelerations are the result of discontinuous left and right motor control force (i.e., f_1 and f_2), as shown in Fig. 8 for case 1. Note that the forces converge to their steady state value to keep the velocity of the USV equal

https://doi.org/10.1017/S0263574710000585 Published online by Cambridge University Press

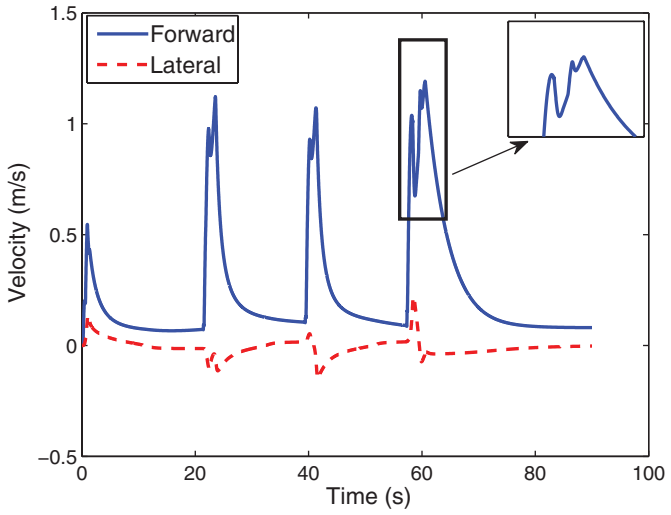

Fig. 6. The forward and lateral velocities of the USV in case 1.

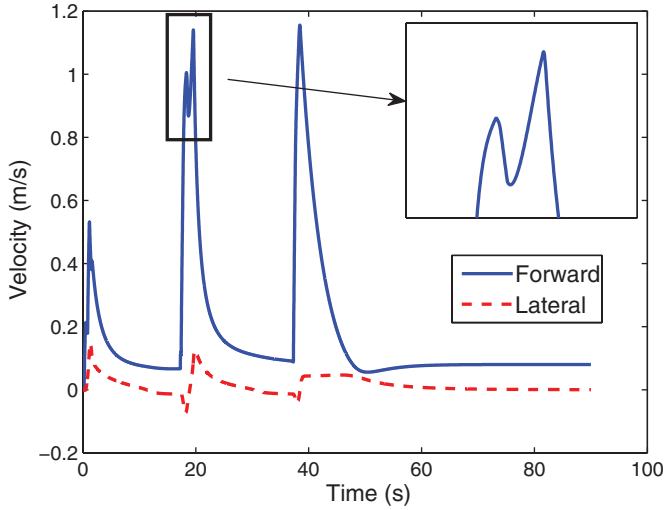

Fig. 7. The forward and lateral velocities of the USV in case 2.

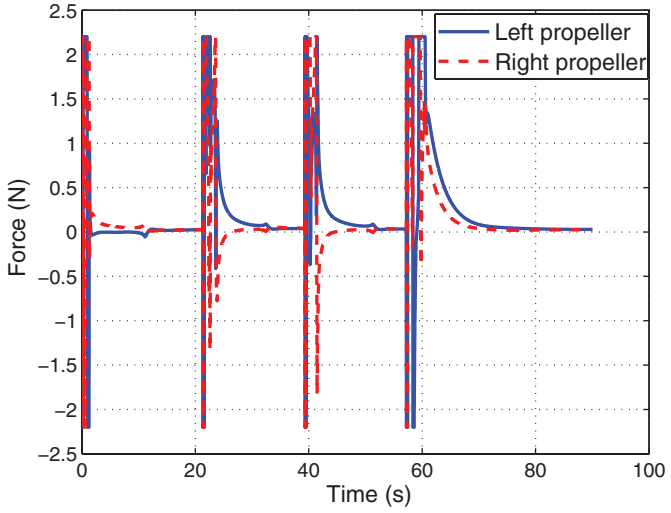

Fig. 8. The control forces of the two USV propellers in case 1.

Table IV. Experimental obstacle size and position data..

	Obstacle #1	Obstacle #2	Obstacle #3
x_o	0.554	2.30	2.70
y_o	1.378	1.75	3.00
a	0.75	0.50	0.50
b	0.75	0.25	0.25
ϕ_o	0	$\pi/3$	0

to the target's constant velocity when the target is reached. The large control action arises because the sliding mode control law does not directly control the heading angle, which results in oscillations at the beginning of each trajectory, as shown in Fig. 9 for case 1. It may be possible to reduce the heading angle oscillations through careful selection of the control parameters[26] and smoother parameter transitions with higher order polynomials to include higher order derivative continuity. However, design of a new control formulation to include heading angle oscillation reduction may be the best option.

4.2. Experimental example

In this case, a simpler example with static obstacles is considered due to our experimental setup size limitation. The pool is 3.05-m wide, 4.88-m long, and 1.22-m deep. A color camera is installed at approximately 3 m above the center of the pool to capture the position and orientation of the USV, obstacle position and size, and the target position. The pool is calibrated using light-emitting diodes (LEDs) similar to the procedure in ref. [7]. Different color LEDs are installed near the two ends of the USV and the target and specific locations on the obstacles. Hence, each image captured by the camera can be filtered to determine the USV feedback data (x, y, θ), target position (x_t, y_t), and obstacle data (x_o, y_o, a, b, ϕ_o); the feedback rate is about .06 s, which is used to estimate the velocities.

The hull of the USV (obtained from a toy boat) has a dark blue color and has the properties listed in Table I. The two propellers are actuated by Micromo®-1516 DC motors connected to LEGO Mindstorms NXT controller with Blue tooth communication. Its initial position and orientation is at .984 m and .375 m and 80° above the horizontal, respectively. There are three static obstacles, one larger and square-shaped and two smaller and rectangular-shaped. The data for the ellipses approximating the obstacles are presented in Table IV. The target is identical to the USV with lighter yellow color initially hiding behind the larger obstacle at .56 m and 2.14 m. It stays at its position for 4.75 s and then moves at a constant speed of .104 m/s heading 73.3° above the horizontal.

A period of .5 s is selected for all interpolations required for smooth transition from one trajectory to the next. The trajectory parameters $\bar{k}_1 = \bar{k}_2 = .04$ and $\bar{\Omega} = .2$ are chosen for the limit cycle trajectories and $\bar{k}_1 = \bar{k}_2 = .25$ for the final target trajectory. The sliding mode control parameters are selected as $\eta_1 = \eta_2 = .1$, $\gamma_1 = \gamma_2 = 1$, and $\varphi_1 = \varphi_2 = .01$. Using new experiments, we were able to estimate the saturation limits for the surge control force ($f_{max} = .59$N) and yaw control moment ($T_{max} = .042$Nm).

https://doi.org/10.1017/S0263574710000585 Published online by Cambridge University Press

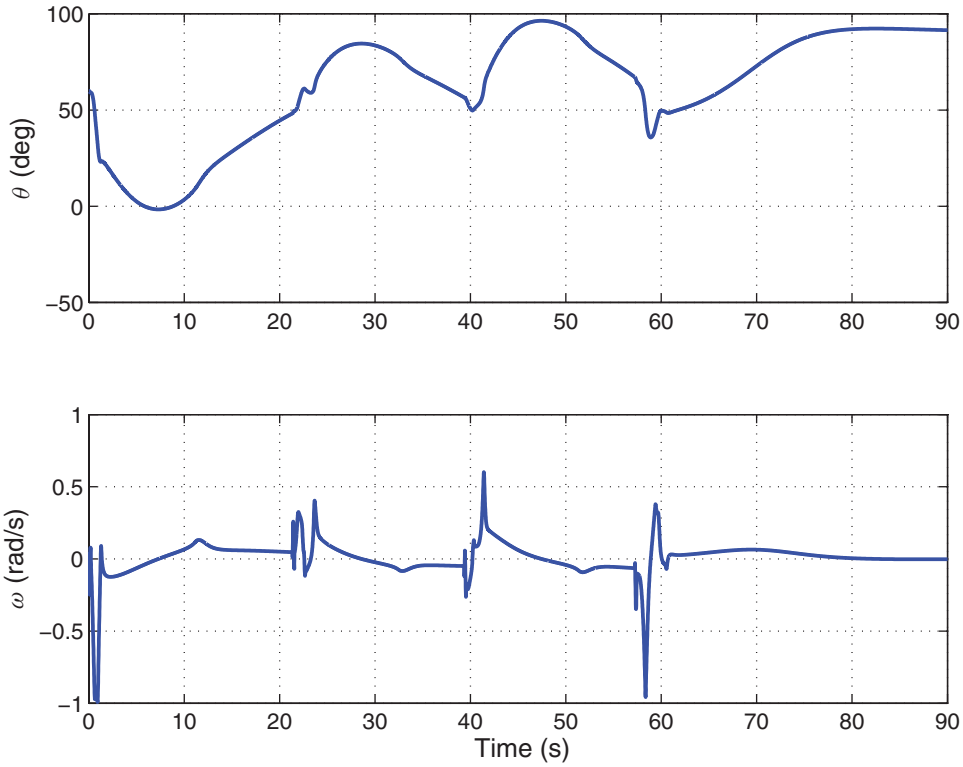

Fig. 9. The heading angle and angular velocity of the USV in case 1.

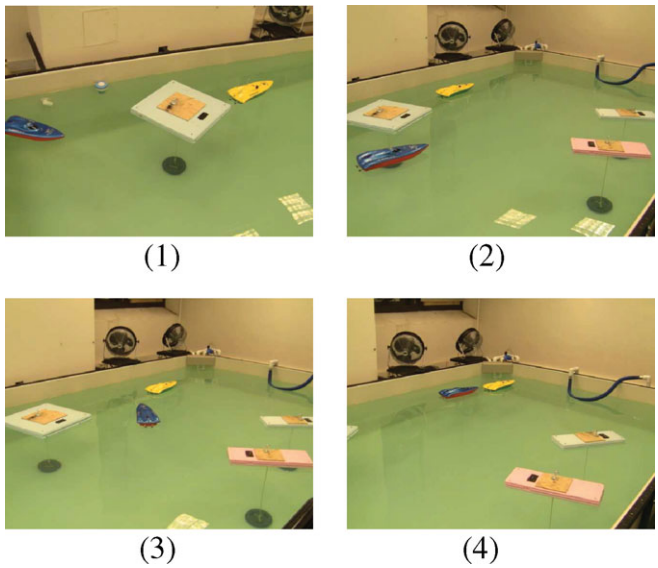

Fig. 10. Four snapshots of the experimental USV (dark blue) catching a moving target (light yellow) in a field of three obstacles.

Figure 10 shows four snapshots of the experiments starting at 1 s after the start (frame 1), at 3 s when it starts going around the limit cycle (frame 2), at 9 s after it changes to the transitional target trajectory (frame 3), and at 18 s when it reaches the target (frame 4). The blue (dark) boat in the figure is the USV and the yellow (light) boat is the target. The white flat square is the large obstacle, while the two yellow flat rectangles are the smaller obstacles. In this example, the USV follows only two transitional trajectories: an elliptical limit cycle around the large obstacle and an exponential one to the target. The two smaller obstacles are ignored by the USV because they never cross its path to the target.

The experiment was recreated in simulation to get an insight into the validity of other simulation results that cannot be tested in our limited experimental setup. Figure 11 shows the time history of the USV distance to the target and the USV heading angle obtained from both experiment and simulation. The distance to target is reduced at a relatively steady rate in simulation. It is reduced very slowly in the experiment until the USV goes around the obstacle and then speeds up to catch the target, thereby reducing the distance at a faster rate during the transitional target trajectory. Heading angle plot shows that the reason for slower rate of distance reduction during the initial limit cycle trajectory is the inability of the experimental USV to make a quick turn. Another difference is that the USV heading angle has not settled in the experiment, although it has settled in the simulation. The simulation, however, shows more oscillation in the heading angle when the USV changes from the limit cycle trajectory to the transitional target trajectory. Figure 12 compares the path followed by the vessel in the experiment with the one obtained through simulation. Although the experiment is successful, it is clear from Figs. 11 and 12 that there are significant differences between simulation and the experiment because of various calibration and modeling uncertainties.[8] The surge control force and yaw control moment calculated from the experiment and simulation are similar but show clear differences, as shown in Fig. 13. Further, yaw moment vanishes in simulation but is actively changing in the experiment. This is due to the fact that the heading angle has not settled in the

https://doi.org/10.1017/S0263574710000585 Published online by Cambridge University Press

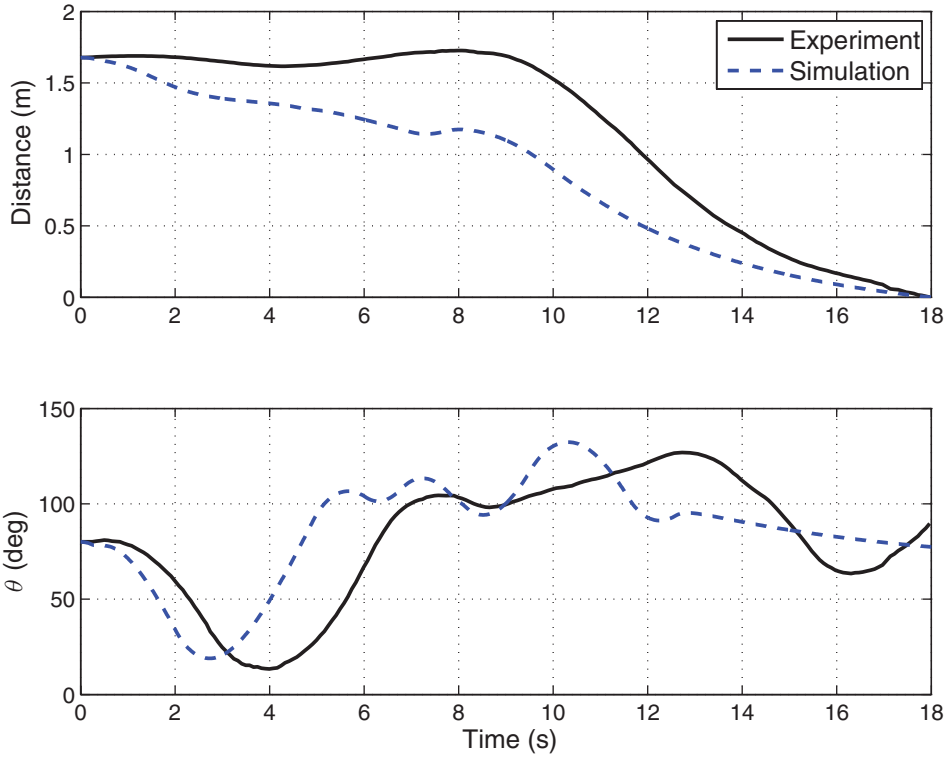

Fig. 11. Comparison of experimental and simulation results: (top) USV distance to target; (bottom) heading angle.

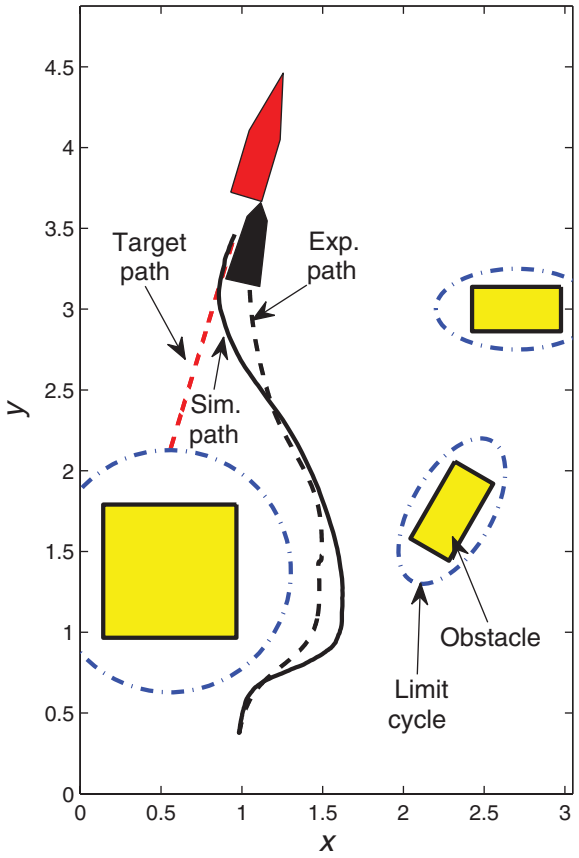

Fig. 12. Comparison of the vessel's path in simulation and experiments.

experiment, as explained above. Figure 14 shows the experimental velocities obtained through finite difference approximation of the position derivatives and kinematic transformation in Eq. (25). The velocity profiles in these figures show a very smooth transition except for small amplitude high-frequency measurement noise, which should be ignored.

5. Conclusions

A new method for obstacle avoidance and trajectory planning of underactuated surface vessels combined with real-time tracking control is developed. A procedure is introduced to continuously detect obstacles, approximate them as ellipses, and plan and track transitional trajectories around them until the target is reached. The transitional trajectories are defined using ODEs whose solutions are stable elliptical limit cycles approximating the obstacles. The last transitional trajectory that will take the vessel to its target is also generated using exponentially stable ODEs. Time-dependent parameters are used for the ODEs and transitions from one trajectory to the next to ensure smooth and practical generation of trajectory. The tracking control law guaranteeing convergence is based on nonlinear sliding mode control, which has been shown to be suitable for real-time implementation and robust to disturbances and modeling uncertainties. Successful simulation with dynamic obstacles and experiment with static ones catching a dynamic target are presented. Future work will include developing a 3D model, experimenting with wind and wave disturbances, and improving the controller design to include actuator saturation and for reduced heading angle oscillation.

https://doi.org/10.1017/S0263574710000585 Published online by Cambridge University Press

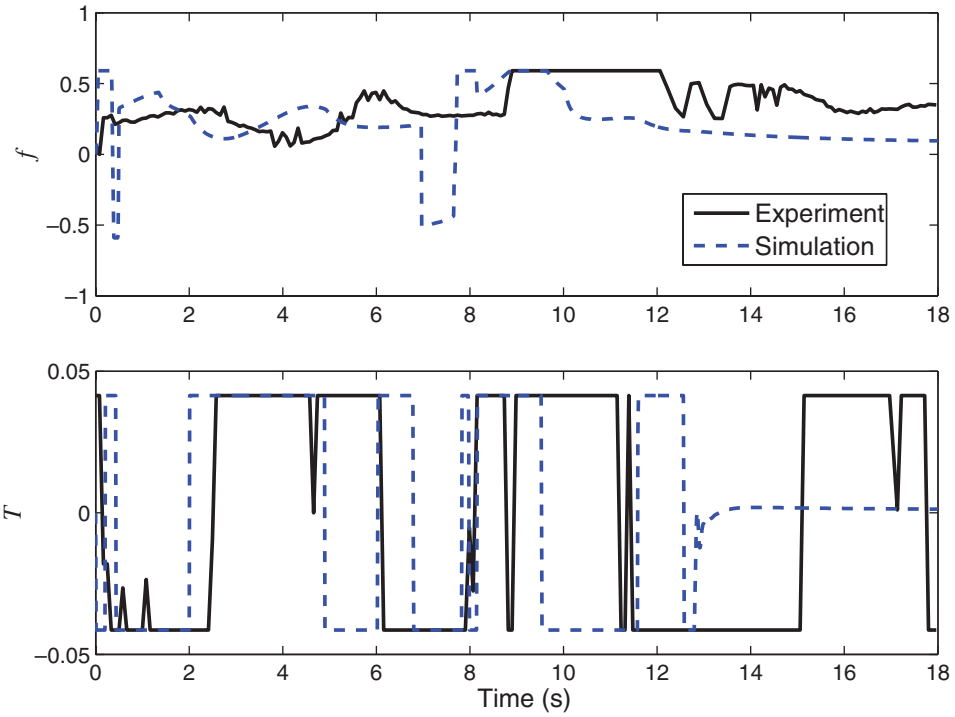

Fig. 13. Comparison of surge force (top) and yaw moment (bottom) control laws obtained during the experiment and simulation.

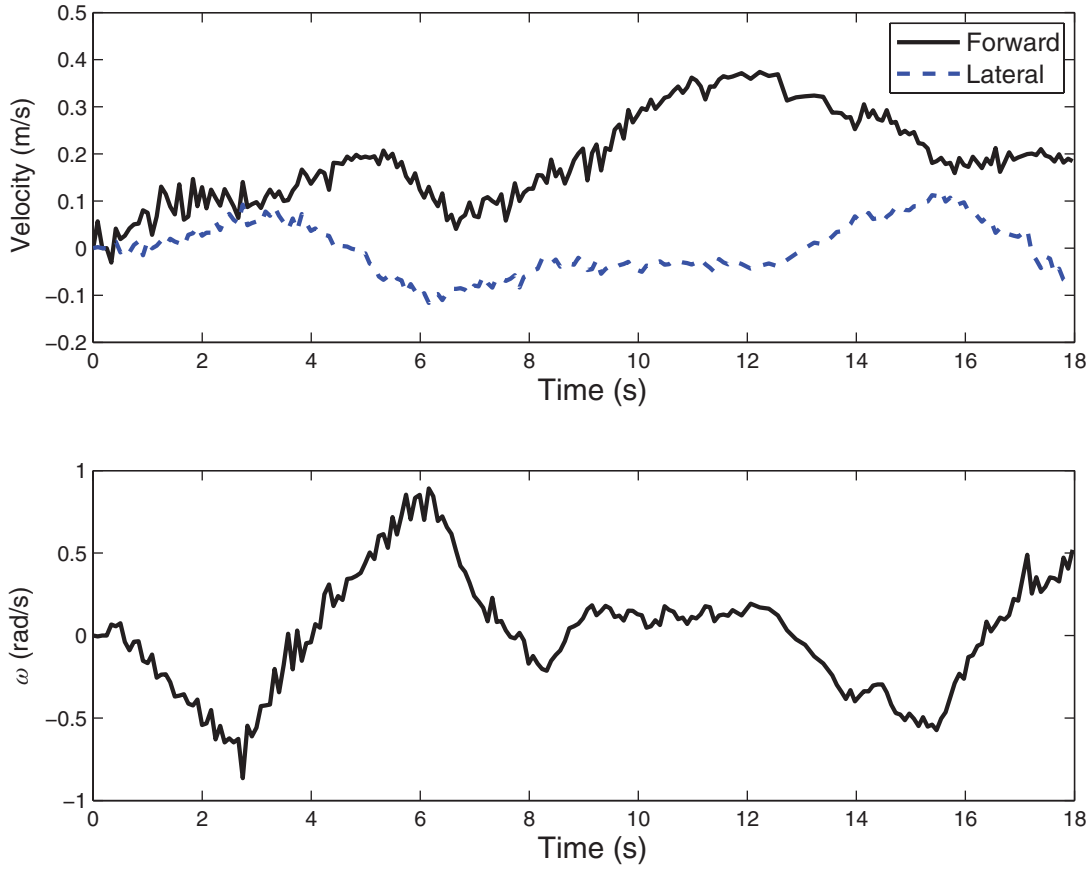

Fig. 14. Experimental forward and lateral velocity (top), angular velocity (bottom).

https://doi.org/10.1017/S0263574710000585 Published online by Cambridge University Press

Acknowledgments

This research was partially supported by the Office of Naval Research under the ONR Grant number N00014-04-1-0642. Support for this work from the Center for Nonlinear Dynamics and Control (CENDAC) at Villanova University is also acknowledged.

References

1. T. I. Fossen, *Guidance and Control of Ocean Vehicles* (John Wiley, New York, NY, 1994).
2. A. Behal, D. M. Dawson, W. E. Dixon and Y. Fang, "Tracking and regulation control of an underactuated surface vessel with nonintegrable dynamics," *IEEE Trans. Autom. Control* **47**(3), 495–500 (2002).
3. J. Godhavn, "Nonlinear Tracking of Underactuated Surface Vessels," *Proceedings of the IEEE Conference on Decision and Control*, Kobe, Japan, vol. 1 (Dec. 11–13, 1996) pp. 975–980.
4. H. Sira-Ramirez, "Dynamic second-order sliding mode control of the hovercraft vessel," *IEEE Trans. Control Syst. Technol.* **10**(6), 860–865 (2002).
5. E. Lefeber, K. Y. Pettersen and H. Nijmeijer, "Tracking control of an underactuated ship," *IEEE Trans. Control Syst. Technol.* **11**(1), 52–61 (2003).
6. A. P. Aguiar and J. P. Hespanha, "Position tracking of underactuated vehicles," *Proc. Am. Control Conf.* **3**, 1988–1993 (2003).
7. K. Y. Peterson, F. Mazenc and H. Nijmeijer, "Global uniform asymptotic stabilization of an underactuated surface vessel: Experimental results," *IEEE Trans. Control Syst. Technol.* **12**(6), 891–903 (2004).
8. H. Ashrafiuon, K. R. Muske, L. McNinch and R. Soltan, "Sliding model tracking control of surface vessels," *IEEE Trans. Ind. Electron.* **55**(11), 4004–4012 (2008).
9. M. Defoort, T. Floquet, A. Kokosy and W. Perruquetti, "A novel higher order sliding mode control scheme," *Syst. Control Lett.* **58**(2), 102–108 (2009).
10. J. Larson, M. Bruch, R. Haiterman, J. Rogers and R. Webster, "Advances in Autonomous Obstacle Avoidance for Unmanned Surface Vehicles," *AUVSI Unmanned Systems*, *North America*, Washington, DC (Aug. 6–9, 2007).
11. K. Fujimura and H. Samet, "A hierarchical strategy for path planning among moving obstacles," *IEEE Trans. Robot. Autom.* **5**(1), 61–69 (1989).
12. N. Aggarwal and K. Fujimura, "Motion Planning Amidst Planar Moving Obstacles," *IEEE International Conference on Robotics and Automation*, San Diego, CA, vol. 3 (May 8–13, 1994) pp. 2153–2158.
13. W. Xiaohua, V. Yadav and S. N. Balakrishnan, "Cooperative UAV formation flying with obstacle/collision avoidance," *IEEE Trans. Control Syst. Technol.* **15**(4), 672–679 (2007).
14. A. R. Dieguez, R. Sanz and J. Lopez, "Deliberative on-line local path planning for autonomous mobile robots," *J. Intell. Robot. Syst.: Theor. Appl.* **37**(1), 1–19 (2003).
15. S. G. Zavlangasand Tzafestas, "Motion control for mobile robot obstacle avoidance and navigation: A fuzzy logic-based approach," *Syst. Anal. Model. Simul.* **43**(12), 1625–1637 (2003).
16. A. Ferrara and M. Rubagotti, "Second-order sliding-mode control of a mobile robot based on a harmonic potential field," *IET Control Theor. Appl.* **2**(9), 807–818 (2008).
17. J. Kim and P. K. Khosla, "Real-time obstacle avoidance using harmonic potential functions," *IEEE Trans. Robot. Autom.* **3**, 338–349 (1992).
18. S. S. Ge and Y. J. Cui, "Dynamic motion planning for mobile robots using potential field method," *Autom. Robot.* **1**, 207–222 (2002).
19. F. A. Cosio and M. P. Castaneda, "Autonomous robot navigation using adaptive potential fields," *Math. Comput. Model.* **40** (9–10), 1141–1156 (2004).
20. K. Pathak and S. K. Agrawal, "An integrated path-planning and control approach for nonholonomic unicycles using switched local potentials," *IEEE Trans. Robot.* **21**(6), 1201–1208 (2005).
21. F. Fahimi, C. Nataraj and H. Ashrafiuon, "Real-time obstacle avoidance for multiple mobile robots," *Robotica* **27**(2), 189–198 (2009).
22. L. P. Ellekilde and J. W. Perram, "Tool center trajectory planning for industrial robot manipulators using dynamical systems," *Int. J. Robot. Res.* **24**(5), 385–396 (2005).
23. D. H. Kim and J. H. Kim, "A real-time limit-cycle navigation method for fast mobile robots and its application to robot soccer," *Robot. Auton. Syst.* **42**(1), 17–30 (2003).
24. D. H. Kim and P. Chongkug, "Limit Cycle Navigation Method for Mobile Robot," *27th Chinese Control Conference*, Kunming, Yunnan, China (July 16–18, 2008) pp. 320–324.
25. R. Grech and S. G. Fabri, "Trajectory Tracking in the Presence of Obstacles using the Limit Cycle Navigation Method," *IEEE International Symposium on Intelligent Control* and *the 13th Mediterranean Conference on Control and Automatio*n, Limassol, Cyprus (June 27–29, 2005) pp. 101–106.
26. R. A. Soltan, H. Ashrafiuon and K. R. Muske, "State-Dependent Trajectory Planning and Tracking Control of Unmanned Surface Vessels," *American Control Conference*, St. Louis, MO (June 10–12, 2009) pp. 3597–3602.
27. A. Ghaffari, M. Tomizuka and R. A. Soltan, "The stability of limit cycles in nonlinear systems," *Nonlinear Dyn.* **56**(3), 269–275 (2008).
28. M. Nikkhah, H. Ashrafiuon and K. Muske, "Optimal Sliding Mode Control for Underactuated Systems," *American Control Conference*, Minneapolis, MN (June 14–16, 2006) pp. 4688–4693.
29. K. Muske, H. Ashrafiuon, G. Haas, R. McCloskey and T. Flynn, "Identification of a Control Oriented Nonlinear Dynamic USV Model," *American Control Conference*, Seattle, WA (June 11–13, 2008) pp. 562–567.
30. V. I. Utkin, "Variable structure systems with sliding modes," *IEEE Trans. Autom. Control* **22**, 212–222 (1977).
31. J. Y. Hung, W. Gao and J. C. Hun, "Variable structure control: A survey," *IEEE Trans. Ind. Electron.* **40**(1), 2–22 (1993).
32. H. K. Khalil, *Nonlinear Systems* (Prentice-Hall, Upper Saddle River, NJ, 1996) pp. 552–579.
33. M. Nikkhah and H. Ashrafiuon, "Robust Control of a Vessel Using Camera Feedback and Extended Kalman Filter," Paper No. IMECE2006-16164, *Proceedings of ASME IMECE*, Chicago, IL (Nov. 5–10, 2006).